Manuscript prepared for Atmos. Chem. Phys.
with version 2015/09/17 7.94 Copernicus papers of the LATEX class copernicus.cls.
Date: 10 June 2016

A biogenic CO_2 flux adjustment scheme for the mitigation of large-scale biases in global atmospheric CO_2 analyses and forecasts

A. Agustí-Panareda[1], S. Massart[1], F. Chevallier[2], G. Balsamo[1], S. Boussetta[1], E. Dutra[1], and A. Beljaars[1]

[1]European Centre for Medium-Range Weather Forecasts, Reading, UK
[2]Laboratoire des Sciences du Climat et l'Environnement, Gif-sur-Yvette, France

Correspondence to: A. Agustí-Panareda (anna.agusti-panareda@ecmwf.int)

Abstract. Forecasting atmospheric CO_2 daily at the global scale with a good accuracy like it is done for the weather is a challenging task. However, it is also one of the key areas of development to bridge the gaps between weather, air quality and climate models. The challenge stems from the fact that atmospheric CO_2 is largely controlled by the CO_2 fluxes at the surface, which are difficult to constrain with observations. In particular, the biogenic fluxes simulated by land surface models show skill in detecting synoptic and regional-scale disturbances up to sub-seasonal time-scales, but they are subject to large seasonal and annual budget errors at global scale, usually requiring a posteriori calibration. This paper presents a scheme to diagnose and mitigate model errors associated with biogenic fluxes within an atmospheric CO_2 forecasting system. The scheme is an adaptive calibration referred to as Biogenic Flux Adjustment Scheme (BFAS) and it can be applied automatically in real time throughout the forecast. The BFAS method generally improves the continental budget of CO_2 fluxes in the model by combining information from three sources: (1) retrospective fluxes estimated by a global flux inversion system, (2) land-use information, (3) simulated fluxes from the model. The method is shown to produce enhanced skill in the daily CO_2 10-day forecasts without requiring continuous manual intervention. Therefore, it is particularly suitable for near-real-time CO_2 analysis and forecasting systems.

1 Introduction

Earth-observing strategies focusing on carbon cycle systematic monitoring from satellites, flask and in situ networks (Ciais et al., 2014; Denning et al., 2005) are leading to an increasing number of near-real-time observations available to systems such as those developed in the framework of the European Union Copernicus Atmosphere Monitoring Service (CAMS). CAMS uses the Numerical Weather Prediction (NWP) Integrated Forecasting system for Composition (C-IFS) of the European Centre for Medium range Weather Forecasts (ECMWF) to produce near-real-time global atmospheric composition analysis and forecasts, including CO_2 (Agustí-Panareda et al., 2014) along with other environmental and climate relevant tracers (Flemming et al., 2009; Morcrette et al., 2009; Massart et al., 2014). The purpose of the real-time CO_2 analysis/forecasting system is to provide timely products that can be used by the scientific community among other users. For example, those working on new instruments, field experiments, satellite retrieval products, regional models requiring boundary conditions, or planning flight campaigns.

The present monitoring of global atmospheric CO_2 relies on observations of atmospheric CO_2 from satellites – e.g. Greenhouse Gases Observing Satellite (GOSAT, www.gosat.nies.go.jp); Orbiting Carbon Observatory 2 (OCO-2, oco.jpl.nasa.gov) – and flask and in situ networks – e.g. National Oceanic and Atmospheric Administration Earth System Research Laboratory (NOAA/ESRL, www.esrl.noaa.gov/gmd); Integrated Carbon Observation System (ICOS, icos-atc.lsce.ipsl.fr); Environment Canada (www.ec.gc.ca/mges-ghgm) – which are assimilated by global tracer transport models to infer changes in atmospheric CO_2 (e.g. Massart et al., 2015) or by flux inversion systems (e.g. Peylin et al., 2013) to estimate the large-scale surface fluxes of CO_2.

The current C-IFS CO_2 analysis is produced by assimilating CO_2 data retrieved from GOSAT by the University of Bremen (Heymann et al., 2015), as well as all the meteorological data that is routinely assimilated in the operational meteorological analysis at ECMWF. Massart et al. (2015) have shown that the atmospheric data assimilation system alone cannot completely remove the biases in the background

atmospheric CO_2 associated with the accumulation of errors in the CO_2 fluxes from the model. This happens because currently the CO_2 surface fluxes in the IFS data assimilation system cannot be constrained by observations. The model biases in atmospheric CO_2 also present a problem for the data assimilation system because its optimisation relies on the assumption that both model and observations are unbiased. It is therefore imperative to remove any large biases before assimilating observations. In this paper, we present a method to reduce the atmospheric CO_2 model biases by adjusting the CO_2 surface fluxes in a near-real-time CO_2 analysis/forecasting system, such as the one used by C-IFS at ECMWF.

Many different methods already exists to adjust CO_2 fluxes by using observations of atmospheric CO_2 within flux inversion systems (Rödenbeck et al., 2003; Gurney et al., 2003; Peters et al., 2007). However, these are not all suitable for the C-IFS real-time monitoring system. Flux inversion systems adjust the fluxes by either inferring the model parameters in Carbon Cycle Data Assimilation Systems also known as CCDAS (Rayner et al., 2005; Scholze et al., 2007; Rayner et al., 2011), or the fluxes themselves (Houweling et al., 2015). CCDAS has the advantage of working in prognostic mode once the model parameters have been optimised. Nevertheless, it can also be prone to aliasing information to the wrong model parameter when the processes that contribute to the variability of atmospheric CO_2 are not properly represented in the model or missing altogether. Estimating directly the CO_2 fluxes does not rely on the accurate representation of complex/unknown processes in the CO_2 flux model, but the resulting optimised fluxes do not have predictive skill. Both approaches generally use long data assimilation windows of several weeks to years in order to be able to constrain the global mass of CO_2 by relying mainly on high quality in situ flask and continuous observations which are relatively sparse in time and space. This general requirement for long assimilation windows is incompatible with the current NWP framework (e.g. a 12-h window is currently used in the IFS). In addition to that, the CO_2 observations from flask and most in situ stations used by these flux inversion systems are not available in near-real time.

Considering all the aspects mentioned above, a Biogenic Flux Adjustment Scheme (hereafter called BFAS) suitable for the NWP framework is proposed which aims to combine the best characteristics of both flux inversion approaches. Namely, the mass constraint from the optimised fluxes is used to correct the biases of the modelled CO_2 fluxes while keeping the predictive skill of the modelled fluxes at synoptic scales. The main objective of BFAS is to reduce the large-scale biases of the background atmospheric CO_2. This should improve the representation of the atmospheric CO_2 large-scale gradients, and thereby also lead to a better forecast of atmospheric CO_2 synoptic variability.

The details of the flux adjustment scheme are provided in Sect. 2. Section 3 describes the IFS experiments done to test the impact of BFAS on the atmospheric CO_2 forecast. From the experiments, different aspects of the flux adjustment can be monitored (i.e. the scaling factors and the resulting budget) as shown in Sect. 4. The resulting atmospheric CO_2 forecast fit to observations after applying BFAS is presented in Sect. 5. The potential use of BFAS for model development and the possibility of including BFAS in the data assimilation system are discussed in Sect. 6. Finally, Sect. 7 gives a summary of the flux adjustment achievements and possible developments for the future.

2 Methodology

Any atmospheric CO2 analysis/forecast system requires a flux adjustment of some sort in order to constrain the budget of sources/sinks a the surface and avoid the growth of mean errors in the atmospheric background (Agustí-Panareda et al., 2014). The scientific question addressed in this paper is how to use the best information we have in near-real time to adjust the fluxes in a way that reduces the bias of the atmospheric CO_2 in the model with the minimum deterioration of the synoptic skill to predict day-to-day variability.

Agustí-Panareda et al. (2014) documented the configuration of the CO_2 forecasting system and showed that the large biases in atmospheric CO_2 are consistent with errors associated with the budget of CO_2 surface fluxes, in particular the Net Ecosystem Exchange (NEE) modelled by the CTESSEL carbon model (Boussetta et al., 2013) within the C-IFS.

There are three main reasons for modelling NEE fluxes online as opposed to using offline fluxes such as optimized fluxes from flux inversion systems directly in the model: (i) the coupling of CO_2 biogenic fluxes with the atmospheric model can lead to improvements in both the understanding of interactions between ecosystems and the evolution of CO_2 in the atmospheric boundary layer (Lu et al., 2001; Moreira et al., 2013) and the forecast skill of energy and water cycle fluxes in NWP models (Boussetta et al., 2013); (ii) the use of offline fluxes would entail a loss of information and the introduction of topographical inconsistencies when downscaling fluxes from low resolution (e.g. typically a few degrees in optimized fluxes) to high resolution (e.g. currently 9 km in ECMWF NWP model); (iii) the non-availability of these offline fluxes in near-real time implies the interannual variability of the NEE fluxes (Schaefer. et. al., 2002) cannot be represented.

The challenge remains of how to reduce the large-scale biases associated with the modelled fluxes in real time. Because these biogenic fluxes are modelled online, a one-off scaling of the fluxes using a climatology of the annual global budget (Nassar et al., 2010; Chen et al., 2013) or re-scaling locally the NEE in order to get a better fit with the seasonal cycle (Messerschmidt et al., 2013; Keppel-Aleks et al., 2012) are not suitable methods, as we do not know the annual budget of the model in real-time.

Optimised fluxes from flux inversion systems constitute the best available estimate of the CO_2 fluxes given the observed variations of CO_2 in the atmosphere at global scales. Thus, they can provide a reference benchmark for the modelled fluxes. The large-scale biases in the CO_2 fluxes can be diagnosed by computing the budget (i.e. integrated) differences between modelled fluxes and optimised fluxes over continental and supra-synoptic spatial and temporal scales (≥ 1000 km, 10 days). Working with budgets over scales beyond the synoptic scale allows the detection of large-scale biases without interfering with the synoptic skill of the model.

It is important to note that there are uncertainties and limitations that should be considered when using optimised fluxes. Optimised fluxes are computed with flux inversion systems at low resolutions ($\sim$ hundreds of km) compared to the NWP resolution used for the CO_2 forecasts ($\sim$ tens of km), and they are most reliable at continental and supra-synoptic scales. Moreover, they have the limitation of not being available in near-real time, unlike the meteorological observations or CO_2 satellite retrievals (Massart et al., 2015). Because of that, a climatology of the optimised fluxes has to be used as a reference.

Finally, optimised fluxes only provide information on the total CO_2 flux because flux inversion systems are not able to attribute the CO_2 variability to the different processes controlling the fluxes, such as vegetation, anthropogenic sources and fires. Generally, from all these fluxes, the land CO_2 fluxes from vegetation and soils in models are associated with high uncertainty (Le Quéré et al., 2015). For this reason, the Global Carbon Project provides the CO_2 budget from land vegetation – also known as the land sink – as a residual to close the carbon budget (see www.globalcarbonproject.org/carbonbudget). Following the land sink residual approach, the optimised NEE can be computed as the residual of optimised fluxes by subtracting the other prescribed fluxes. A set of 10-day mean budgets of this residual NEE from optimised fluxes is then computed daily for different regions and vegetation types over a period of 10 years to build the NEE climatology that can be used as a reference. In order to account for the inter-annual variability of NEE, the reference climatology is also adjusted with an inter-annual variability factor obtained from the model.

The flux adjustment scheme essentially estimates the bias of the modelled NEE budget with respect to the reference NEE budget for each region and vegetation type as a scaling factor α:

$$\alpha = \frac{f^{\mathrm{O}}}{f^{\mathrm{M}}} \qquad (1)$$

where f is the 10-day mean NEE budget computed daily over a specific vegetation type and region, f^{O} is the reference budget based on the MACC-13R1 optimised fluxes (Chevallier et al., 2010), and f^{M} is the budget of the modelled fluxes. Figure 1 shows how the BFAS scheme interacts with the model to produce the flux-corrected atmospheric CO_2 fore-

cast. First of all, the uncorrected NEE fluxes from the model are retrieved. Then their budget is compared with the budget of the NEE climatology from the optimised fluxes adjusted with the NEE anomaly from the model. The scheme produces maps with scaling factors of the biogenic fluxes before the forecast run. Subsequently, these maps are then used to scale the forecast of NEE. There are three major building blocks required for the computation of these scaling factors:

- The computation of the NEE budget using temporal and spatial aggregation criteria (e.g. 10 days, vegetation types, different regions).

- A reference NEE dataset used to diagnose the model biases (e.g. optimised fluxes from global flux inversion systems such as the MACC-13R1 dataset from Chevallier et al. (2010)).

- The partition of the NEE adjustment into the two modelled ecosystem fluxes that make up the NEE flux: i.e. Gross Primary Production (GPP) associated with photosynthesis and ecosystem respiration (R_{eco}) documented by Boussetta et al. (2013).

These different aspects are discussed in further detail below in Sect. 2.1 to 2.4.

2.1 Computation of NEE budget

The biases of the NEE fluxes that we aim to correct are partly linked to model parameter errors that depend on vegetation type and to errors in the meteorological/vegetation state which are region-dependent (e.g. radiation, LAI, temperature and precipitation). In addition to that, the global optimised fluxes used as reference do not currently have a strong constraint from observations at small spatial and temporal scales due to the sparse observing network of atmospheric CO_2. Therefore, the NEE biases are not diagnosed at the model grid-point scale, but as biases in the NEE budget over continental regions for different vegetation types and over a period of 10 days. The 10-day regional budget provides an indicator on the large-scale biases. Moreover, 10 days is a period that can be used in the current framework of the C-IFS global atmospheric CO_2 forecasting system. Figure 2 shows how the uncorrected NEE from the past forecasts can be combined to compute the 10-day mean budget before each new forecast. The 1-day forecasts initialised from the previous seven days are used together with the last 3-day forecast available in order to create a 10-day window around the initial date of the new forecast. This 10-day time window is slightly shifted to the past because otherwise forecasts longer than 3-days would be required to compute the budget while errors in the meteorology affecting the fluxes grow with forecast lead time. Chevallier and Kelly (2002) found that forecast errors associated with the location of extra-tropical weather systems affecting the cloud cover and temperature gradients – which in turn will affect the NEE errors – are very small

at day 1. These errors continue to be small up to day 3, but they can grow rapidly with forecast lead time (see Haiden et al., 2015, for details on the IFS forecast error evaluation). The different regions have been selected according to latitudinal band characterised by seasonal cycle (northern hemisphere, tropics and southern hemisphere), continental region and vegetation type.

In the IFS the vegetation types follow the BATS classification (Dickinson et al., 1986), which is widely used in meteorological and climate models. The vegetation classification is designed to distinguish between roughness lengths for the computation of the momentum, heat and moisture transfer coefficients in the modelling of the fluxes from surface to atmosphere. However, the BATS vegetation types are not always suitable for the modelling of the CO_2 fluxes. For example, the interrupted forest type which constitutes around 25 % of the high vegetation cover encompasses many different types of vegetation, including Tropical Savanna and a combination of remnants of forest or open woods lands with field complexes. This could be an important source of error in some regions. For this reason, BFAS allows the introduction of new vegetation types for diagnosing the NEE biases. Tropical Savanna which covers large areas in the tropical region has been added as a subtype of the interrupted forest vegetation type by using the Olson Global Ecosystem classification (Olson, 1994a, b, edc2.usgs.gov/glcc/globdoc2_0.php).

Figure 3 shows the distribution of the dominant vegetation types used in BFAS. Land cover maps from GLCC version 1 (edc2.usgs.gov/glcc/glcc.php) are used to compute the land cover of the dominant high and low vegetation types at each grid point. In BFAS, only one dominant vegetation type is used to classify each grid point, and this must cover more than 50 % of the grid box. Model grid points with less than 50 % vegetation cover are not used. The comparison of the modelled NEE with the optimised NEE fluxes is done by computing 10-day budgets for each of the 16 vegetation types (see Table 1) and 9 different regions (see Fig. 3).

2.2 Reference NEE budget

The residual NEE from optimised fluxes provides the reference for the flux adjustment scheme. Currently, there is no operational centre providing CO_2 optimised fluxes at global scale in near-real time. We have chosen to use the MACC optimised fluxes (Chevallier et al., 2010) which are delivered around September each year for the previous year. The MACC optimised CO_2 fluxes are regularly improved and their high quality has been recently shown by Kulawik et al. (2015). Chevallier (2013) provides an evaluation of the inverted CO_2 fluxes for 2010.

The computation of the residual is done by subtracting the prescribed fluxes used in the C-IFS CO_2 forecast over land from the total optimised flux. The prescribed CO_2 fluxes from biomass burning and anthropogenic emissions in the CO_2 forecast are not the same as the ones used as prior fluxes in the MACC flux inversion system. Not only they are from different sources, but they are also used at different resolutions. This means that there might be fires represented in one and not the other, or with different emission intensities, as it is the case for anthropogenic hotspots at high versus low resolutions. Thus, in order to avoid the transfer of inconsistencies between the prescribed and prior fluxes into the NEE residual, the regions with very high anthropogenic emissions (larger than $3 \times 10^6 \, \text{g C m}^{-2} \, \text{s}^{-1}$) and fires are filtered out.

A climatology of these reference NEE fluxes is created using the last 10 available years and it is updated every time a new year is available. Thus, allowing for slow decadal variations in the NEE reference. Figure 4 shows a comparison of the optimised flux budget in 2010 and its climatology for the crop vegetation type in North America. The inter-annual variability of the optimised flux budget is depicted by the standard deviation around the 10-year climatology. The reference NEE climatology is then adjusted to account for the inter-annual variability of the land sink fluxes as follows:

$$f^{\text{O}} = f^{\text{Oclim}} + \gamma \sigma \left(f^{\text{Oclim}} \right), \qquad (2)$$

where f is the 10-day NEE budget for a specific region and vegetation type, f^{O} is the reference budget, f^{Oclim} and $\sigma(f^{\text{Oclim}})$ are the climatological mean and standard deviation of the optimised flux budget respectively from 2004 to 2013, and γ is the corresponding standardised anomaly of the NEE budget from the model with respect to the same period. γ can be positive or negative. It represents the inter-annual variability factor used to adjust the reference climatological NEE budget and it is given by

$$\gamma = \frac{f^{\text{M}} - f^{\text{Mclim}}}{\sigma \left(f^{\text{Mclim}} \right)} \qquad (3)$$

where f^{M} is the model NEE budget, f^{Mclim} is the climatological mean budget from the model and $\sigma(f^{\text{Mclim}})$ is the standard deviation of the model NEE budget denoting the typical amplitude of its inter-annual variability for the same period as the climatology of the optimised flux budget (i.e. 2004 to 2013).

The γ inter-annual variability factor is multiplied by the standard deviation of the optimised residual NEE budget – representing the typical amplitude of inter-annual variability – in order to offset the reference climatological NEE budget. In this way, the inter-annual variability of the reference NEE follows the inter-annual variability of the model NEE with the same anomaly sign, while keeping its amplitude constrained by the standard deviation of the optimised flux budget. Note that the use of this factor is optional. By setting it to zero, the model budget can be constrained by the optimized flux climatology. The rationale for applying this factor in the C-IFS system is based on the fact that inter-annual variability of the NEE budget is strongly linked to the inter-annual variability of climate variables such as precipitation and temperature (Schaefer et. al., 2002). Since information on these

climate variables is readily available in the C-IFS system, it is worth exploring its impact on the CO_2 forecast. A preliminary assessment of the impact of including the inter-annual variability factor was performed by comparing experiment with and without the factor. Results confirmed a small but positive impact (see Supplement). Details on the computation of this factor are given in the next section.

2.3 The inter-annual variability factor

The computation of the inter-annual variability factor γ requires a model climate consistent with the forecast (i.e. same meteorological analysis, same model version and same resolution). Producing a consistent model climate is not a trivial requirement, because both the operational model version and analysis system can change frequently with new updates and new observations, and high resolution forecasts spanning a period of 10 years (i.e. 2004 to 2013) are expensive. A feasible solution has been found where the standardised NEE anomaly from the model is computed using the operational Ensemble Prediction System (ENS) forecasts and hindcasts which are part of the ECMWF monthly forecasting system (Vitart et al., 2008; Vitart, 2013, 2014). Every Monday and Thursday the operational ENS is not only run for the actual date, but also for the same calendar day of the past 20 years. These hindcasts have the same resolution and model version as the ENS forecasts and they constitute a valuable data set used for the post-processing and calibration of the NWP forecasts from the medium-range (10 days) up to one month lead times (Hagedorn et al., 2012). The ensemble of forecasts is made of 5 members (10 members since 2015) using perturbed initial conditions (Lang et al., 2015) and stochastic physics in order to represent forecast uncertainty (Palmer et al., 2009).

As the hindcasts are not performed daily, it is not possible to aggregate consecutive 1-day forecasts into a 10-day period to compute a mean budget as shown in Fig. 2. In order to circumvent this, the mean budget is computed by averaging the 1-day forecast NEE from all the ensemble members available in the hindcasts. This is done for each year from 2004 to 2013 to preserve consistency with the NEE climatology from the optimised fluxes. The model climate f^{Mclim} given by the 10-year mean budget and its typical inter-annual variability $\sigma\left(f^{\mathrm{Mclim}}\right)$ can then be obtained by calculating the mean value and standard deviation respectively over that period. Similarly, the model budget f^{M} is calculated from the NEE ensemble mean of the ENS forecast for the current date using the same number of ensemble members as the ENS hindcasts. The standardised anomaly γ is finally obtained by subtracting the 10-year mean budget from the current budget and dividing the anomaly by the standard deviation. Since the hindcasts are available every Monday and Thursday, γ is only updated twice a week. These updates are routinely monitored during the forecast (see Sect. 4).

2.4 Partition of NEE adjustment

The final stage in the flux adjustment is the attribution of the NEE correction to the different biogenic fluxes in the model. The residual NEE from optimised fluxes only provides information on the total flux from the land ecosystem exchange. While in land vegetation models, NEE is the combination of two opposing fluxes: Gross Primary Production (GPP) and the ecosystem respiration (R_{eco}). Given that we have no information on whether the NEE error is associated with the GPP or the R_{eco} fluxes, a strategy has to be defined in order to partition the NEE correction into GPP and R_{eco}. The underlying strategy used here is to have the smallest flux adjustment possible. Namely, the scaling factors should be as close to 1 as possible.

The first step is to distinguish between the positive and negative values of the NEE scaling factor (α). A positive NEE scaling factor implies the budget of the NEE in the model has the correct sign but the wrong magnitude. In that case, the scaling of the flux will be smallest if the dominant component of NEE is scaled. That is to say, the flux correction will be applied to GPP during the growing season and to R_{eco} during the senescence period. Whereas if the scaling factor is negative – i.e. the modelled NEE has the wrong sign – only the flux with smallest magnitude is corrected (GPP or R_{eco}) to ensure the scaling factor of the modelled fluxes is always positive.

The scaling factor α is then converted into a scaling factor for the dominant component of the NEE flux. If the magnitude of GPP is larger than the magnitude of R_{eco}, then the scaling factor for GPP and R_{eco} are defined as follows:

$$
\begin{aligned}
\alpha_{\mathrm{GPP}} &= \frac{\alpha \mathrm{NEE} - R_{\mathrm{eco}}}{\mathrm{GPP}} \\
\alpha_{R_{\mathrm{eco}}} &= 1.0
\end{aligned}
\tag{4}
$$

Similarly, if $|R_{\mathrm{eco}}| > |\mathrm{GPP}|$ then

$$
\begin{aligned}
\alpha_{\mathrm{GPP}} &= 1.0 \\
\alpha_{R_{\mathrm{eco}}} &= \frac{\alpha \mathrm{NEE} - \mathrm{GPP}}{R_{\mathrm{eco}}}
\end{aligned}
\tag{5}
$$

This partition the flux adjustment is a modelling choice based on minimum flux adjustment criteria. Other solutions might be possible given additional information on either GPP or R_{eco} budgets.

The α_{GPP} and $\alpha_{R_{\mathrm{eco}}}$ factors are computed for each vegetation type and region and then re-mapped as 2-d fields using the dominant vegetation type map in Fig. 3. The resulting maps for α_{GPP} and $\alpha_{R_{\mathrm{eco}}}$ are subsequently passed to the carbon module in the land surface model in order to scale GPP and R_{eco}.

3 CO_2 forecast simulations

Several simulations have been performed in order to test the impact of BFAS on the atmospheric CO_2 forecasts (see Table 2). All the simulations use the C-IFS CO_2 forecasting system (Agustí-Panareda et al., 2014) based on the IFS model (www.ecmwf.int/en/forecasts/documentation-and-support). They all share the same transport. The only difference between them is the CO_2 surface fluxes they use as described in Table 2. The impact of BFAS is assessed by comparing the simulations using modelled NEE fluxes without BFAS (CTRL) and with BFAS (BFAS). The BFAS simulation is also compared with the simulations using optimised fluxes (OPT) and a climatology of optimised fluxes (OPT-CLIM). Both OPT and OPT-CLIM simulations constitute a benchmark because they are driven by the reference fluxes used in BFAS. From these experiments we expect to see the forecast from BFAS to be closer to the benchmark forecasts (in particular OPT-CLIM) than to the CTRL forecast.

The forecasts are performed using the cyclic configuration described by Agustí-Panareda et al. (2014) with a spectral resolution of TL255, equivalent to around 80 km in the horizontal, and 60 vertical levels. They are initialised daily at 00:00 UTC with ECMWF operational analysis, while the atmospheric CO_2 is cycled from one forecast to the next, as in a free run. The simulations span the period from 1 January to 31 December 2010. This period has been selected because of the large variety of observations available to evaluate the BFAS performance on the atmospheric CO_2 forecasts. The CO_2 initial conditions on 1 January 2010 are from the atmospheric CO_2 analysis using GOSAT CO_2 retrievals (Heymann et al., 2015).

4   Monitoring the flux adjustment

The flux adjustment is monitored by plotting time series of the flux scaling factors for each vegetation type and region. For example, Fig. 5 shows the GPP and R_{eco} scaling factors for the crop vegetation type which is present in all regions. The values range from 0.5 to 6. These coefficients are computed daily before the beginning of each forecast and they are kept constant throughout the forecast. Generally, there is a slow variation of the coefficients from one day to the next. This is expected since the coefficients are obtained from large-scale budgets computed over a 10-day period. The map of the GPP and R_{eco} scaling factors applied to adjust the modelled biogenic fluxes on 15 March 2010 is shown in Fig. 6. These maps can be very useful to monitor the flux adjustment because they can provide alerts on the regions with largest biases to model developers.

The effect of the flux adjustment on the NEE budget is shown in Fig. 7. The adjusted biogenic fluxes should always lead to an NEE budget close to the budget of the optimised NEE climatology. However, the fit will also depend on the degree of inter-annual variability of the model determined by parameter γ in Eq. (3). Figure 8 displays the monitoring of γ given by the standardised NEE anomaly of the model. Positive values mean the CO_2 source is larger than normal and/or the CO_2 sink is lower than normal with respect to the 10-year mean budget of the model, covering the same period as the reference climatology. Conversely, negative values correspond to a smaller than normal source and/or larger than normal sink. When γ is larger than 1, the model anomaly is larger than 1σ. This indicates the possible occurrence of an extreme event. Prolonged extreme events – such as droughts – would have an effect on the NEE budget and the computation of the biogenic flux adjustment.

5   Impact of the flux adjustment

The impact of BFAS is shown by comparing the atmospheric CO_2 from the BFAS forecast to the CTRL forecast, and to the benchmark forecasts with optimised fluxes (OPT and OPT-CLIM) at several observing sites. Four sites from the NOAA/ESRL atmospheric baseline observatories (www.esrl.noaa.gov/gmd/obop, Thoning et al., 2012) are used to evaluate the reduction of the large-scale biases in the well-mixed background air. In addition, four Total Carbon Column Observing Network stations (GGG2014 TCCON data, Wunch et al., 2011, see Table 3 and www.tccon.caltech.edu) are also used to assess the impact on the atmospheric CO_2 column-average dry molar fraction. Finally, three continental sites from the NOAA/ESRL tall tower network (www.esrl.noaa.gov/gmd/ccgg/towers, Andrews et al., 2014) are used to investigate the impact of BFAS on the synoptic skill of the forecasts. The results are grouped into the impacts on bias reduction and synoptic skill in the following two sections. A comprehensive evaluation of the uncertainty reduction in the BFAS simulation based on all the **?** in situ flask and continuous observations, as well as the NOAA/ESRL aircraft vertical profiles (Sweeney et al., 2015) is also provided in the Supplement.

5.1   Biases in atmospheric CO_2

Figure 9 demonstrates that BFAS is very effective at reducing the atmospheric CO_2 biases in the background air at all the NOAA/ESRL continuous baseline stations. The biases in the CTRL forecast range from -1.9 to -4.5 ppm; whereas, the BFAS forecast has biases of -0.5 ppm or less over the whole year. These values are close to the annual biases of the OPT and OPT-CLIM experiments ranging between -0.4 and 0.5 ppm. The monthly biases in BFAS can be larger than its annual biases. For example, there is a bias of up to -1 ppm from March to September in the southern hemisphere (Fig. 9c, d). This bias is thought to originate in the tropical regions and transported to the southern hemi-

sphere as shown by a preliminary comparison with IASI CO_2 (Crevoisier et al., 2009) (not shown here). The bias starts to grow at the end of the growing season during summer time. This is also the case for the high latitude station at Barrow, where there is a negative bias of a few ppm from the last week of July to the end of September as shown in Fig. 9a. In summary, BFAS is not able to completely remove the negative model bias at the end of the growing season. In the northern hemisphere at the end of winter and throughout spring (from March to May) there is a positive model bias, i.e. the atmospheric CO_2 is overestimated in the model. Although the OPT and OPT-CLIM simulations also have a slight positive bias in winter, this positive bias is enhanced in the BFAS simulation.

At the TCCON sites (Fig. 10), the atmospheric CO_2 column-average dry molar fraction also shows the same large bias reduction in BFAS with respect to CTRL. The magnitude of the BFAS annual biases in the atmospheric column is generally less than 1 ppm, slightly higher than the OPT and OPT-CLIM biases (less than 0.5 ppm), but much lower than the CTRL biases (from 1.5 to 3.3 ppm). The results at the TCCON sites are consistent with those from the NOAA/ESRL baseline sites. Namely, in the northern hemisphere there is a growing overestimation of the atmospheric CO_2 at the end of winter (around March). While at the end of the growing season in both northern and southern hemispheres (August and March respectively) there is a growing negative bias, i.e. an overestimation of the sink. One hypothesis that could explain why BFAS is not able to achieve as small a bias as the forecast with optimised fluxes lies in the fact that the optimised NEE used as a reference in BFAS is computed as a residual after removing the effect of fires and anthropogenic fluxes. Inconsistencies in the fire and anthropogenic emissions used by the optimised fluxes and the model will lead to errors in the optimised residual NEE. These inconsistencies are mainly associated with the use of different resolutions. Further investigation is required to address this issue.

5.2 Synoptic variability of atmospheric CO_2

The CO_2 forecast has been shown to have high skill in simulating the synoptic variability of atmospheric CO_2 (see Agustí-Panareda et al., 2014), except during the spring months, coinciding with an early start of the CO_2 drawdown period in the model. For this reason, we have examined the impact of BFAS on the synoptic variability of daily mean atmospheric CO_2 at three continental NOAA/ESRL tower sites in March. Over this period, the day-to-day variability of atmospheric CO_2 at those sites is associated with the advection of atmospheric CO_2 by baroclinic synoptic weather systems as they impinge on the large-scale continental gradient of atmospheric CO_2. Table 4 clearly demonstrates that with BFAS the synoptic forecast skill is greatly improved at all sites, with correlation coefficients between simulated and observed atmospheric CO_2 exceeding 0.8. The improvement

is particularly striking at Park Falls (Wisconsin, USA) and West Branch (Iowa, USA) at the centre of North America, where the correlation coefficients in CTRL are very low (i.e. below 0.5). The OPT and OPT-CLIM forecasts have generally high correlation coefficients, comparable to BFAS. Only at the level closest to the surface, the values are slightly lower than BFAS. This can be explained by the fact that the MACC-13R1 optimised fluxes do not comprise synoptic variability. Thus, when the synoptic variability of the fluxes contributes to the atmospheric CO_2 variability, the correlation coefficients are smaller.

The positive impact of BFAS on the CO_2 synoptic variability is illustrated in Fig. 11. The large synoptic variability is characterised by the advection of CO_2-rich anomalies (with up to 10 ppm amplitude) as shown by the CO_2 peaks on 10–12 March at Park Falls, and 8–9, 12–13 and 16–17 March at West Branch. These CO_2 anomalies originate from the advection across the large-scale continental gradients of atmospheric CO_2 which ultimately reflect the large-scale distribution of CO_2 surface fluxes (Keppel-Aleks et al., 2012). In the case study here, the CO_2-rich air is located to the south of the observing stations, as shown by the distribution of the monthly mean atmospheric CO_2 depicting the large-scale gradients across the continent at the level corresponding to the height of the tall towers (Figs. 12a and 12b). In the CTRL forecast, there is no monthly mean gradient south of the stations (Fig. 12c). This explains why without BFAS the synoptic variability is very small and largely underestimated throughout March. While in BFAS the gradient south of the observing stations is very pronounced (Fig. 12d), following a similar pattern to OPT and OPT-CLIM. There are still some differences between the three simulations. OPT-CLIM results in stronger gradients than OPT and BFAS enhances the gradient even further, leading to a slight overestimation of the synoptic variability. These differences in the patterns of the atmospheric CO_2 are directly linked to the differences in the CO_2 surface fluxes (Fig. 13). As expected, the flux adjustment from BFAS results in a flux pattern similar to OPT-CLIM and OPT, with a stronger source to the south of the observing stations. Whereas in CTRL there is a large sink area south of the observing stations, in the region of the Gulf of Mexico, consistent with the CTESSEL early growing season (Balzarolo et al., 2014).

6 Discussion

All the results from the BFAS experiments indicate that BFAS is highly beneficial to the C-IFS CO_2 forecasting system, both in terms of reducing the atmospheric CO_2 biases and improving the synoptic skill of the model. As shown in Sect. 2, the scheme is simple and it is easy to implement and run. Because BFAS essentially works as a layer on top of the model, it can adapt to model changes with great flexibility.

For all these reasons, BFAS is now part of the operational global C-IFS analysis and forecasting system.

Notwithstanding all the advantages of BFAS listed above, there are also caveats that need to be considered, further tested and addressed. A discussion of the current limitations of BFAS is provided in this section, together with the potential use of BFAS for model development, data assimilation purposes and the implications for users.

6.1 Current limitations in BFAS

Optimised fluxes have uncertainties of their own and represent the large-scale variability of the CO_2 surface fluxes on supra-synoptic time-scales. They only estimate the total flux and the NEE residual approach can transfer biases from other fluxes into the NEE. The use of a climatology also precludes the correction of the inter-annual variability in the model.

The aggregation criteria of budget errors can be very challenging because the error can originate from different aspects of the model. Clearly, errors in model parameters associated with vegetation type are a good candidate. However, in the future errors in climate forcing, errors in LAI, missing processes and other potential sources of error should also be considered.

The partition of the NEE flux adjustment into the modelled biogenic fluxes (GPP and R_{eco}) is currently ad-hoc, leading to the transfer of errors from GPP to R_{eco} and vice-versa. This problem could be addressed by using other independent datasets of GPP and R_{eco} (e.g. Jung et al., 2011) that contain additional information on how to partition the NEE adjustment.

6.2 BFAS for model development

BFAS can run in both online and offline modes. Thus, it can provide a tool to diagnose regions that contribute to the errors in the global budget resulting in large-scale errors of atmospheric CO_2. The maps of biogenic flux scaling factors can be used to compute maps of flux adjustment (e.g. adjusted NEE – original NEE) which can then be used to diagnose model errors. The synthesis of the mean adjustments into monthly model biases for different vegetation types can then guide the effort to develop the carbon model further. For example, in regions where the bias is consistent between different months, the corrected NEE could be used to re-tune model parameters such as the reference ecosystem respiration or the mesophyll conductance, previously optimised by Boussetta et al. (2013) using a subset of FLUXNET data. Specific vegetation types can be identified where model improvements could be achieved by using information from BFAS. For instance, crops have the same large R_{eco} scaling (> 1.5) over all the northern hemisphere regions during winter months when the ecosystem respiration is the dominant component of NEE. This underestimation in the ecosystem respiration can be addressed by modifying the value of the

reference respiration parameter used for crops. In this case, the same procedure used by Boussetta et al. (2013) could be applied to optimise the specific model parameter using the BFAS adjusted fluxes as pseudo-observations together with the FLUXNET data.

Further information on error sources in fluxes can be obtained by comparing the corrected fluxes with the eddy covariance observations available in near-real time from the Integrated Observation System (ICOS) Ecosystem Thematic Centre (ETC, http://www.europe-fluxdata.eu). For example, preliminary comparisons have shown that there are large differences in the model-observation fit between needle leaf evergreen (pine) trees in the boreal and Mediterranean regions. This is consistent with results from Balzarolo et al. (2014), and it highlights the need for a new sub-classification of the evergreen needle leaf forests in regions with Mediterranean climate.

6.3 BFAS in the data assimilation framework

Currently, BFAS is only designed to be used as a bias correction computed before each forecast by using a reference data set based on optimised fluxes. In the future, BFAS could be adapted to work within a data assimilation (DA) framework in the IFS. To start with, the specification of uncertainties associated with both the reference data set and the model fluxes and the covariance of those uncertainties would allow a more optimal estimation of the flux adjustment. These uncertainties can be obtained from the flux inversion systems for the optimised fluxes and from the ECMWF ENS forecasts for the model fluxes.

Including BFAS in the IFS DA framework needs further exploration. The IFS uses a short time window (currently 12 h) to assimilate meteorological observations from very dense observing networks. With the short time window it is not possible to properly constrain the slowly varying global mass of the long-lived greenhouse gases due to the sparseness of their observing system. For instance, the current GOSAT and OCO-2 CO_2 observations do not cover high latitudes in winter. However, if we combined the assimilation of optimised fluxes (which already contain the global mass constraint) with observations linked to local fluxes (e.g. solar-induced chlorophyll fluorescence products from satellites, NEE eddy covariance observations and in situ atmospheric CO_2 observations) it might be possible to obtain an optimal estimate of more local scaling factors, while still respecting the global mass constraint. The possibility of optimising the scaling factors in the DA system within the weak constraint framework (Trémolet, 2006, 2007) also needs to be explored in the future.

6.4 Aspects to be considered by users

The implementation of BFAS is straightforward. Therefore, it could be easily used by other models. The only require-

ments are: (i) a reference budget which can be obtained from a climatology of optimized fluxes (e.g. the MACC product can be easily obtained from www-lscedods.cea.fr/invsat/PYVAR14_MACC/V2/Fluxes/3Hourly and it is well documented); (ii) past 10-day NEE simulated by the forward model; (iii) the NEE anomaly of the forward model with respect to its climate based on a 10-year simulation. The use of the NEE anomaly is optional, as its impact is relatively small (see Supplement).

The underlying motivation of BFAS is to improve the CO_2 analysis and forecast for users (e.g. those working on flux inversion systems, planning field experiments, or requiring boundary conditions for regional models). For this reason, it is paramount to provide information on all the input data going into BFAS. These are primarily continental-scale climatological budgets from modelled NEE and optimized fluxes. There is also some input from the anthropogenic emissions and the biomass burning emissions to extract the NEE as a residual from the optimized fluxes. The documentation of the specific components used in the C-IFS BFAS system and their uncertainties can be found in Boussetta et al. (2013), Chevallier et al. (2010); Chevallier (2015), Janssens-Maenhout et al. (2012) and Kaiser et al. (2012). The input data streams used in BFAS can be obtained from http://copernicus-support.ecmwf.int for C-IFS NEE and GFAS biomass burning fluxes; from the EDGAR database http://edgar.jrc.ec.europa.eu for the anthropogenic fluxes; and from www-lscedods.cea.fr/invsat/PYVAR14_MACC/V2/Fluxes/3Hourly for the MACC optimized fluxes.

Since the BFAS product contains information from the optimized fluxes, users should be aware that the optimized fluxes assimilated most available background air-sample monitoring sites (listed in the supplement of Chevallier (2015), see http://www.atmos-chem-phys.net/15/11133/2015/acp-15-11133-2015-supplement.pdf). A specification of the overall uncertainty associated with the BFAS simulation and the resulting reduction with respect to the control simulation is given in the Supplement.

7 Summary

This paper addresses the challenge of designing an online bias correction for an atmospheric CO_2 analysis/forecasting system. The overarching aim is to deliver an atmospheric CO_2 analysis and forecast that can be useful to the scientific community, e.g. working on data assimilation of atmospheric CO_2 observations, the development of the CO_2 observing system and providing boundary conditions for CO_2 regional modelling. Tunning model parameters and/or rescaling fluxes offline are not sufficient to garantee a bias reduction in the system. Thus, an online adaptive system is required because errors in the meteorology can evolve as a result of regular operational NWP model upgrades and these

affect the NEE budget in the model. This is achieved in the new biogenic flux adjustment scheme (BFAS) by a simple scaling of the 10-day NEE budgets for different vegetation types and regions using a climatology of the MACC optimised fluxes (Chevallier et al., 2010) as a reference, adjusted to preserve the model inter-annual variability.

This paper shows that BFAS has a positive impact on the atmospheric CO_2 forecast by greatly reducing the atmospheric CO_2 biases in background air and improving the synoptic variability in continental regions affected by ecosystem fluxes. The improvement in the synoptic skill of the forecast is associated with underlying changes in the large-scale gradient of the NEE fluxes where optimised fluxes provide information.

BFAS has been recently implemented in the C-IFS operational CO_2 forecast and analysis system, because of its simplicity, adaptability to model changes and beneficial impact. In this paper, the C-IFS model is just providing an example on how this method can be applied efficiently in an operational forecasting system. Other models could easily adopt such as system as there are only a few components required for its implementation (see section 6.4).

As a diagnostic tool, BFAS has also the potential to provide feedback for model development. The use of BFAS in the data assimilation framework will be explored in the future.

Acknowledgements. This study has been funded by the European Commission under the Monitoring of Atmospheric Composition and Climate (MACC) project and the Copernicus Atmosphere Monitoring Service (CAMS).

TCCON data were obtained from the TCCON Data Archive, hosted by the Carbon Dioxide Information Analysis Center (CDIAC) – tccon.onrl.gov. The authors would like to acknowledge the PIs of the different TCCON stations used in this study: Rigel Kivi (Sodankylä, Finland), Nicholas Deutscher (Bialystok, Poland), Paul Wennberg (Lamont, USA) and David Griffith (Wollongong, Australia).

We acknowledge Ed Dlugokencky and Arlene Andrews (NOAA/ESRL) for the NOAA/ESRL data. The NOAA/ESRL Global Monitoring Division data from the baseline observatories at Barrow (Alaska, USA), Mauna Loa (Hawaii, USA), American Samoa (USA), South Pole (Antarctica), as well as the tall towers at Argyle (Maine, USA), Park Falls (Wisconsin, USA) and West Branch (Iowa, USA) were obtained from ftp://aftp.cmdl.noaa.gov/data/greenhouse_gases/co2. We acknowledge Colm Sweeney (NOAA/ESRL) for the NOAA/ESRL aircraft profiles and all the laboratories contributing to the compilation of ?.

The authors are very grateful to Nils Wedi for his support in processing the Olson ecosystem classification maps and to Frederic Vitard for providing support and advice on the use of the ENS hindcasts. We would also like to acknowledge the comments from Peter Rayner and an anonymous reviewer which helped improve the message and documentation of the atmospheric CO2 error reduction associated with the flux adjustment presented in the paper.

References

Agustí-Panareda, A., Massart, S., Chevallier, F., Boussetta, S., Balsamo, G., Beljaars, A., Ciais, P., Deutscher, N. M., Engelen, R., Jones, L., Kivi, R., Paris, J.-D., Peuch, V.-H., Sherlock, V., Vermeulen, A. T., Wennberg, P. O., and Wunch, D.: Forecasting global atmospheric CO$_2$, Atmos. Chem. Phys., 14, 11959–11983, doi:10.5194/acp-14-11959-2014, 2014.

Andrews, A. E., Kofler, J. D., Trudeau, M. E., Williams, J. C., Neff, D. H., Masarie, K. A., Chao, D. Y., Kitzis, D. R., Novelli, P. C., Zhao, C. L., Dlugokencky, E. J., Lang, P. M., Crotwell, M. J., Fischer, M. L., Parker, M. J., Lee, J. T., Baumann, D. D., Desai, A. R., Stanier, C. O., De Wekker, S. F. J., Wolfe, D. E., Munger, J. W., and Tans, P. P.: CO$_2$, CO, and CH$_4$ measurements from tall towers in the NOAA Earth System Research Laboratory's Global Greenhouse Gas Reference Network: instrumentation, uncertainty analysis, and recommendations for future high-accuracy greenhouse gas monitoring efforts, Atmos. Meas. Tech., 7, 647–687, doi:10.5194/amt-7-647-2014, 2014.

Balzarolo, M., Boussetta, S., Balsamo, G., Beljaars, A., Maignan, F., Calvet, J.-C., Lafont, S., Barbu, A., Poulter, B., Chevallier, F., Szczypta, C., and Papale, D.: Evaluating the potential of large-scale simulations to predict carbon fluxes of terrestrial ecosystems over a European Eddy Covariance network, Biogeosciences, 11, 2661–2678, doi:10.5194/bg-11-2661-2014, 2014.

Boussetta, S., Balsamo, G., Beljaars, A., Agusti-Panareda, A., Calvet, J.-C., Jacobs, C., van den Hurk, B., Viterbo, P., Lafont, S., Dutra, E., Jarlan, L., Balzarolo, M., Papale, D., and van der Werf, G.: Natural carbon dioxide exchanges in the ECMWF Integrated Forecasting System: Implementation and offline validation, J. Geophys. Res.-Atmos., 118, 1–24, doi:10.1002/jgrd.50488, 2013.

Chen, Z. H., Zhu, J. and Zeng, N. : Improved simulation of regional CO$_2$ surface concentrations using GEOS-Chem and fluxes from VEGAS, Atmospheric Chemistry and Physics, 13 , 7607–7618, doi:10.5194/acp-13-7607-2013, 2013.

Chevallier, F., On the statistical optimality of CO$_2$ atmospheric inversions assimilating CO$_2$ column retrievals, Atmospheric Chemistry and Physics, 15, 11133–11145, doi:10.5194/acp-15-11133-2015, 2015.

Chevallier, F.: Report on the quality of the inverted CO$_2$ fluxes, MACC-II delivrable D_043.4, ECMWF, available at: http://www.gmes-atmosphere.eu/documents/maccii/deliverables/ghg/MACCII_GHG_DEL_D43.4_20120430_Chevallier.pdf (last access: 21 December 2015), 2013.

Chevallier, F. and Kelly, G.: Model clouds as seen from space: comparison with geostationary imagery in the 11-m window channel, Mon. Weather Rev., 130, 712–722, 2002.

Chevallier, F., Ciais, P., Conway, T., Aalto, T., Anderson, B., Bousquet, P., Brunke, E., Ciattaglia, L., Esaki, Y., Fröhlich, M., Gomez, A., Gomez Pelaez, A., Haszpra, L., Krummel, P., Langenfelds, R., Leuenberger, M., Machida, T., Maignan, F., Matsueda, H., Morgu, J., Mukai, H., Nakazawa, T., Peylin, P., Ramonet, M., Rivier, L., Sawa, Y., Schmidt, M., Steele, L., Vay, S., Vermeulen, A., Wofsy, S., and Worthy, D.: CO$_2$ surface fluxes at grid point scale estimated from a global 21 year reanalysis of atmospheric measurements, J. Geophys. Res., 115, D21307, doi:10.1029/2010JD013887, 2010.

Crevoisier C., Chédin A., Scott N. A., Matsueda H., Machida T., and Armante R., First year of upper tropospheric integrated content of CO2 from IASI hyperspectral infrared observations, Atmos. Chem. Phys., 9, 4797-4810, 2009.

Ciais, P., Dolman, A. J., Bombelli, A., Duren, R., Peregon, A., Rayner, P. J., Miller, C., Gobron, N., Kinderman, G., Marland, G., Gruber, N., Chevallier, F., Andres, R. J., Balsamo, G., Bopp, L., Bréon, F.-M., Broquet, G., Dargaville, R., Battin, T. J., Borges, A., Bovensmann, H., Buchwitz, M., Butler, J., Canadell, J. G., Cook, R. B., DeFries, R., Engelen, R., Gurney, K. R., Heinze, C., Heimann, M., Held, A., Henry, M., Law, B., Luyssaert, S., Miller, J., Moriyama, T., Moulin, C., Myneni, R. B., Nussli, C., Obersteiner, M., Ojima, D., Pan, Y., Paris, J.-D., Piao, S. L., Poulter, B., Plummer, S., Quegan, S., Raymond, P., Reichstein, M., Rivier, L., Sabine, C., Schimel, D., Tarasova, O., Valentini, R., Wang, R., van der Werf, G., Wickland, D., Williams, M., and Zehner, C.: Current systematic carbon-cycle observations and the need for implementing a policy-relevant carbon observing system, Biogeosciences, 11, 3547–3602, doi:10.5194/bg-11-3547-2014, 2014.

Denning, S., Oren, R., McGuire, D., Sabine, C., Doney, S., Paustian, K., Torn, M., Dilling, L., Heath, L., Tans, P., Wofsy, S., Cook, R., Waltman, S., Andrews, A., Asner, G., Baker, J., Bakwin, P., Birdsey, R., Crisp, D., Davis, K., Field, C., Gerbig, C., Hollinger, D., Jacob, D., Law, B., Lin, J., Margolis, H., Marland, G., Mayeux, H., McClain, C., McKee, B., Miller, C., Pawson, S., Randerson, J., Reilly, J., Running, S., Saleska, S., Stallard, R., Sundquist, E., Ustin, S., and Verma, S.: Science implementation strategy for the North American Carbon Program, Report on the NACP Implementation Strategy Group of the U.S. Carbon Cycle Interagency Working Group, Washington, DC, USA, U.S. Carbon Cycle Science Program, 2005.

Deutscher, N., Notholt, J., Messerschmidt, J., Weinzierl, C., Warneke, T., Petri, C., Grupe, P., and Katrynsk, K.: TCCON data from Bialystok, Poland, Release GGG2014R0., Tech. rep., TCCON data archive, hosted by the Carbon Dioxide Information Analysis Center, Oak Ridge National Laboratory, Oak Ridge, Tennessee, USA., doi:10.14291/tccon.ggg2014.bialystok01.R0/1149277, 2014.

Dickinson, R., Henderson-Sellers, A., Kennedy, P., and Wilson, M. F.: Biosphere-atmosphere transfer scheme (BATS) for the NCAR community model, Ncar technical note, NCAR, nCAR/TN-275+STR NOAA, doi:10.5065/D6668B58, 1986.

Flemming, J., Inness, A., Flentje, H., Huijnen, V., Moinat, P., Schultz, M. G., and Stein, O.: Coupling global chemistry transport models to ECMWF's integrated forecast system, Geosci. Model Dev., 2, 253–265, doi:10.5194/gmd-2-253-2009, 2009.

Griffith, D. W. T., Velazco, V. A., Deutscher, N., Murphy, C., Jones, N., Wilson, S., Macatangay, R., Kettlewell, G., Buchholz, R. R., and Riggenbach, M.: TCCON data from Wollongong, Australia, Release GGG2014R0, Tech. rep., TCCON data archive, hosted by the Carbon Dioxide Information Analysis Center, Oak Ridge National Laboratory, Oak Ridge, Tennessee, USA, doi:10.14291/tccon.ggg2014.wollongong01.R0/1149291, 2014.

Gurney, K., Law, R., Denning, A., Rayner, P., Baker, D., Bousquet, P., Bruhwiler, L., Chen, Y.-H., Ciais, P., Fan, S., Fung, I., Gloor, M., Heimann, M., Higuchi, K., John, J., Maki, T., Maksyutov, S., Masarie, K., Peylin, P., Prather, M., Pak, B., Sarmiento, J., Taguchi, S., Takahashi, T., and Yuen, C.-W.: TransCom3 CO$_2$ inversion intercomparison: 1. Annual mean control results and

sensitivity to transport and prior flux information, Tellus B, 55, 555–579, 2003.

Hagedorn, R., Buizza, R., Hamill, M., Leutbecher, M., and Palmer, T.: Comparing TIGGE multi-model forecasts with re-forecast calibrated ECMWF ensemble forecasts, Q. J. R. Meteor. Soc., 138, 1814–1827, 2012.

Haiden, T., Janousek, M., Bauer, P., Bidlot, J., Dahoui, M., Ferranti, L., Prates, F., Richardson, D., and Vitart, F.: Evaluation of ECMWF forecasts, including 2014–2015 upgrades, Technical Report 765, ECMWF, available at: www.ecmwf.int/en/elibrary/miscellaneous/14691-evaluation-ecmwf-forecasts-including-2014-2015-upgrades (last access: 5 January 2016), 2015.

Heymann, J., Reuter, M., Hilker, M., Buchwitz, M., Schneising, O., Bovensmann, H., Burrows, J. P., Kuze, A., Suto, H., Deutscher, N. M., Dubey, M. K., Griffith, D. W. T., Hase, F., Kawakami, S., Kivi, R., Morino, I., Petri, C., Roehl, C., Schneider, M., Sherlock, V., Sussmann, R., Velazco, V. A., Warneke, T., and Wunch, D.: Consistent satellite XCO2 retrievals from SCIAMACHY and GOSAT using the BESD algorithm, Atmos. Meas. Tech., 8, 2961–2980, doi:10.5194/amt-8-2961-2015, 2015.

Houweling, S., Baker, D., Basu, S., Boesch, H., Butz, A., Chevallier, F., Deng, F., Dlugokencky, E. J., Feng, L., Ganshin, A., Hasekamp, O., Jones, D., Maksyutov, S., Marshall, J., Oda, T., O'Dell, C. W., Oshchepkov, S., Palmer, P. I., Peylin, P., Poussi, Z., Reum, F., Takagi, H., Yoshida, Y., and Zhuravlev, R.: An intercomparison of inverse models for estimating sources and sinks of CO_2 using GOSAT measurements, J. Geophys. Res.-Atmos., 120, 5253–5266, doi:10.1002/2014JD022962, 2015.

Janssens-Maenhout, G., Dentener, F., Aardenne, J. V., Monni, S., Pagliari, V., Orlandini, L., Klimont, Z., Kurokawa, J., Akimoto, H., Ohara, T., Wankmueller, R., Battye, B., Grano, D., Zuber, A., and Keating, T.: EDGAR-HTAP: a Harmonized Gridded Air Pollution Emission Dataset Based on National Inventories, JRC68434, EUR report No EUR 25 299-2012, ISBN 978-92-79-23122-0, ISSN 1831-9424, European Commission Publications Office, Ispra, Italy, 2012.

Jung, M., Reichstein, M., Margolis, H. A., Cescatti, A., Richardson, A. D., Arain, M. A., Arneth, A., Bernhofer, C., Bonal, D., Chen, J., Gianelle, D., Gobron, N., Kiely, G., Kutsch, W., Lasslop, G., Law, B. E., Lindroth, A., Merbold, L., Montagnani, L., Moors, E. J., Papale, D., Sottocornola, M., Vaccari, F., and Williams, C.: Global patterns of land-atmosphere fluxes of carbon dioxide, latent heat, and sensible heat derived from eddy covariance, satellite, and meteorological observations, J. Geophys. Res.-Biogeo., 116, G00J07, doi:10.1029/2010JG001566, 2011.

Kaiser, J. W., Heil, A., Andreae, M. O., Benedetti, A., Chubarova, N., Jones, L., Morcrette, J.-J., Razinger, M., Schultz, M. G., Suttie, M., and van der Werf, G. R.: Biomass burning emissions estimated with a global fire assimilation system based on observed fire radiative power, Biogeosciences, 9, 527–554, doi:10.5194/bg-9-527-2012, 2012.

Keppel-Aleks, G., Wennberg, P. O., Washenfelder, R. A., Wunch, D., Schneider, T., Toon, G. C., Andres, R. J., Blavier, J.-F., Connor, B., Davis, K. J., Desai, A. R., Messerschmidt, J., Notholt, J., Roehl, C. M., Sherlock, V., Stephens, B. B., Vay, S. A., and Wofsy, S. C.: The imprint of surface fluxes and transport on variations in total column carbon dioxide, Biogeosciences, 9, 875–891, doi:10.5194/bg-9-875-2012, 2012.

Kivi, R., Heikkinen, P., and Kyro, E.: TCCON data from Sodankyla, Finland, Release GGG2014R0, Tech. rep., TCCON data archive, hosted by the Carbon Dioxide Information Analysis Center, Oak Ridge National Laboratory, Oak Ridge, Tennessee, USA, doi:10.14291/tccon.ggg2014.sodankyla01.R0/1149280, 2014.

Kulawik, S. S., Wunch, D., O'Dell, C., Frankenberg, C., Reuter, M., Oda, T., Chevallier, F., Sherlock, V., Buchwitz, M., Osterman, G., Miller, C., Wennberg, P., Griffith, D. W. T., Morino, I., Dubey, M., Deutscher, N. M., Notholt, J., Hase, F., Warneke, T., Sussmann, R., Robinson, J., Strong, K., Schneider, M., and Wolf, J.: Consistent evaluation of GOSAT, SCIAMACHY, CarbonTracker, and MACC through comparisons to TCCON, Atmos. Meas. Tech. Discuss., 8, 6217–6277, doi:10.5194/amtd-8-6217-2015, 2015.

Lang, S. T. K., Bonavita, M., and Leutbecher, M.: On the impact of re-centring initial conditions for ensemble forecasts, Q. J. R. Meteor. Soc., 141, 2571–2581, 2015.

Le Quéré, C., Moriarty, R., Andrew, R. M., Peters, G. P., Ciais, P., Friedlingstein, P., Jones, S. D., Sitch, S., Tans, P., Arneth, A., Boden, T. A., Bopp, L., Bozec, Y., Canadell, J. G., Chini, L. P., Chevallier, F., Cosca, C. E., Harris, I., Hoppema, M., Houghton, R. A., House, J. I., Jain, A. K., Johannessen, T., Kato, E., Keeling, R. F., Kitidis, V., Klein Goldewijk, K., Koven, C., Landa, C. S., Landschützer, P., Lenton, A., Lima, I. D., Marland, G., Mathis, J. T., Metzl, N., Nojiri, Y., Olsen, A., Ono, T., Peng, S., Peters, W., Pfeil, B., Poulter, B., Raupach, M. R., Regnier, P., Rödenbeck, C., Saito, S., Salisbury, J. E., Schuster, U., Schwinger, J., Séférian, R., Segschneider, J., Steinhoff, T., Stocker, B. D., Sutton, A. J., Takahashi, T., Tilbrook, B., van der Werf, G. R., Viovy, N., Wang, Y.-P., Wanninkhof, R., Wiltshire, A., and Zeng, N.: Global carbon budget 2014, Earth Syst. Sci. Data, 7, 47–85, doi:10.5194/essd-7-47-2015, 2015.

Lu, L., R.A.Pielke, Sr., G.E. Liston, W. Parton, D. Ojima, and M. Hartman: The Implementation of a two-way Interactive Atmospheric and Ecological Model and its Application to the Central United States. Journal of Climate, 14, 900–919, 2001.

Massart, S., Agusti-Panareda, A., Aben, I., Butz, A., Chevallier, F., Crevoisier, C., Engelen, R., Frankenberg, C., and Hasekamp, O.: Assimilation of atmospheric methane products into the MACC-II system: from SCIAMACHY to TANSO and IASI, Atmos. Chem. Phys., 14, 6139–6158, doi:10.5194/acp-14-6139-2014, 2014.

Massart, S., Agustí-Panareda, A., Heymann, J., Buchwitz, M., Chevallier, F., Reuter, M., Hilker, M., Burrows, J. P., Hase, F., Desmet, F., Feist, D. G., and Kivi, R.: Ability of the 4-D-Var analysis of the GOSAT BESD XCO2 retrievals to characterize atmospheric CO_2 at large and synoptic scales, Atmos. Chem. Phys., 16, 1653–1671, doi:doi:10.5194/acp-16-1653-2016, 2016.

Messerschmidt, J., N. Parazoo, D. Wunch, N.M. Deutscher, C. Roehl, T. Warneke and P.O.Wennberg: Evaluation of seasonal atmosphere-biosphere exchange estimations with TCCON measurements, Atmospheric Chemistry and Physics, 13 , 5103-5115, doi:10.5194/acp-13-5103-2013, 2013.

Morcrette, J.-J., J.-J., Boucher, O., Jones, L., Salmond, D., Bechtold, P., Beljaars, A., Benedetti, A., Bonet, A., Kaiser, J., Razinger, M., Schulz, M., Serrar, S., Simmons, A., Sofiev, M., Suttie, M., Tompkins, A., and Untch, A.: Aerosol analysis and forecast in the European Centre for Medium-Range Weather Forecasts Integrated Forecast System: Forward modeling, J. Geophys. Res., 114, D06206, doi:10.1029/2008JD011235, 2009.

Moreira, D. S., Freitas, S. R., Bonatti, J. P., Mercado, L. M., Rosário, N. M. É., Longo, K. M., Miller, J. B., Gloor, M., Gatti, L. V.: Coupling between the JULES land-surface scheme and the CCATT-BRAMS atmospheric chemistry model (JULES-CCATT-BRAMS1.0): applications to numerical weather forecasting and the CO_2 budget in South America, Geoscientific Model Development, 6, 1243–1259, doi:10.5194/gmd-6-1243-2013, 2013.

Nassar, R. and Jones, D. B. A. and Suntharalingam, P. and Chen, J. M. and Andres, R. J. and Wecht, K. J. and Yantosca, R. M. and Kulawik, S. S., Bowman and K. W. and Worden, J. R. and Machida, T. and Matsueda, H. (2010): Modeling global atmospheric CO_2 with improved emission inventories and CO_2 production from the oxidation of other carbon species, Geosci. Model Dev., 3, 689-716, doi:10.5194/gmd-3-689-2010, 2010.

Cooperative Global Atmospheric Data Integration Project; Multi-laboratory compilation of atmospheric carbon dioxide data for the period 1968-2014; obspack_co2_1_GLOBALVIEWplus_v1.0_2015-07-30; NOAA Earth System Research Laboratory, Global Monitoring Division. doi: 10.15138/G3RP42, http://dx.doi.org/10.15138/G3RP42

Olson, J.: Global Ecosystems Framework: Definitions, U.S. Geological Survey, Sioux Falls, SD, USA, 37 pp., 1994a.

Olson, J.: Global Ecosystems Framework: Translation strategy, U.S. Geological Survey, Sioux Falls, SD, USA, 39 p., 1994b.

Palmer, T., Buizza, R., Doblas Reyes, F., Jung, T., Leutbech, M., Shutts, G., Steinheimer, M., and Weisheimer, A.: Stochastic parametrization and model uncertainty, Technical Memorandum 598, ECMWF, ECMWF, Shinfield Park, Reading, RG2 9AX, UK, 2009.

Peters, W., Jacobson, A., Sweeney, C., Andrews, A., Conway, T., Masarie, K., Miller, J., Bruhwiler, L., Petron, G., Hirsch, A., Worthy, D., van der Werf, G., Randerson, J., Wennberg, P., Krol, M., and Tans, P.: An atmospheric perspective on North American carbon dioxide exchange: CarbonTracker, P. Natl. Acad. Sci., 104, 18925–18930, doi:10.1073/pnas.0708986104, 2007.

Peylin, P., Law, R. M., Gurney, K. R., Chevallier, F., Jacobson, A. R., Maki, T., Niwa, Y., Patra, P. K., Peters, W., Rayner, P. J., Rödenbeck, C., van der Laan-Luijkx, I. T., and Zhang, X.: Global atmospheric carbon budget: results from an ensemble of atmospheric CO_2 inversions, Biogeosciences, 10, 6699–6720, doi:10.5194/bg-10-6699-2013, 2013.

Polavarapu, S.M., M. Neish, M. Tanguay, C. Girard, J. de Grandpré, S. Gravel, K. Semeniuk, and D. Chan (2015): Adapting a weather forecast model for greenhouse gas simulation, AGU Fall Metting, San Francisco, 15-18 December 2015, Poster A31B-0037.

Rayner, P., Scholze, M., Knorr, W., Kaminski, T., Giering, R., and Widmann, H.: Two decades of terrestrial carbon fluxes from a carbon cycle data assimilation system (CCDAS), Global Biogeochem. Cy., 19, GB2026, doi:10.1029/2004gb002254, 2005.

Rayner, P., Koffi, E., Scholze, M., Kaminski, T., and Dufresne, J.-L.: Constraining predictions of the carbon cycle using data, P. T. R. Soc. A, 369, 1955–1966, doi:10.1098/rsta.2010.0378, 2011.

Rödenbeck, C., Houweling, S., Gloor, M., and Heimann, M.: CO_2 flux history 1982–2001 inferred from atmospheric data using a global inversion of atmospheric transport, Atmos. Chem. Phys., 3, 1919–1964, doi:10.5194/acp-3-1919-2003, 2003.

Schaefer, K., A.S. Denning, N. Suits, J.Kaduk, I. Baker, S. Losd, and L. Prihodko (2002): Effect of climate on inter-annual variability of terrestrial CO_2 fluxes, Global Biogeochemical Cycles, 16, 2002.

Schepers, D., S. Guerlet, A. Butz, J.Landgraf, C. Frankenberg, O. Hasekamp and J.-F. Blavier, N.M. Deutscher, D.W.T. Griffith and F. Hase, E. Kyro, I. Morino, V. Sherlock, R. Sussmann, and I. Aben: Methane retrievals from Greenhouse Gases Observing Satellite (GOSAT) shortwave infrared measurements: Performance comparison of proxy and physics retrieval algorithms, Journal of Geophysical Research, 117, D10307, doi:10.1029/2012JD017549, 2012.

Scholze, M., Kaminski, T., Rayner, P., Knorr, W., and Giering, R.: Propagating uncertainty through prognostic carbon cycle data assimilation sytem simulations, J. Geophys. Res., 112, D17305, doi:10.1029/2007JD008642, 2007.

Sweeney, C., A. Karion, S. Wolter, T. Newberger, D. Guenther, J. A. Higgs and A. E. Andrews, P. M. Lang, D. Neff, E. Dlugokencky, J. B. Miller and S. A. Montzka, B. R. Miller, K. A. Masarie, S. C. Biraud, P. C. Novelli, M. Crotwell, A. M. Crotwell, K. Thoning, and P. P. Tans: Seasonal climatology of CO2 across North America from aircraft measurements in the NOAA/ESRL Global Greenhouse Gas Reference Network, Journal of Geophysical Research: Atmospheres, 120, 10, doi:10.1002/2014JD022591, 2015.

Takahashi, T., Sutherland, S., Wanninkhof, R., Sweeney, C., Feely, R., Chipman, D., Hales, B., Friederich, G., Chavez, F., Watson, A., Bakker, D., Schuster, U., Metzl, N., Yoshikawa-Inoue, H., Ishii, M., Midorikawa, T., Nojiri, Y., Sabine, C., Olafsson, J., Arnarson, T., Tilbrook, B., Johannessen, T., Olsen, A., Bellerby, R., Krtzinger, A., Steinhoff, T., Hoppema, M., de Baar, H., Wong, C., Delille, B., and Bates, N. R.: Climatological mean and decadal changes in surface ocean pCO_2, and net sea-air CO_2 flux over the global oceans, Deep-Sea Res. II, 56, 554–577, 2009.

Thoning, K., Kitzis, D., and Crotwell, A.: Atmospheric Carbon Dioxide Dry Air Mole Fractions from quasi-continuous measurements at Barrow, Alaska; Mauna Loa, Hawaii; American Samoa; and South Pole, 1973–2011, Version: 2012-05-07, Tech. Rep., NOAA, available at: ftp://aftp.cmdl.noaa.gov/data/greenhouse_gases/co2/in-situ/ (last access: 18 December 2015), 2012.

Trémolet, Y.: Accounting for an imperfect model in 4D-Var, Q. J. R. Meteor. Soc., 132, 2483–2504, 2006.

Trémolet, Y.: Model-error estimation in 4D-Var, Q. J. R. Meteor. Soc., 133, 1267–1280, doi:10.1002/qj.94, 2007.

Vitart, F.: Evolution of ECMWF sub-seasonal forecast skill scores over the past 10 years, Technical Memorandum 694, ECMWF, available at: www.ecmwf.int/en/elibrary/miscellaneous/12932-evolution-ecmwf-sub-seasonal-forecast-skill-scores-over-past-10 (last access: 5 January 2016), 2013.

Vitart, F.: Evolution of ECMWF sub-seasonal forecast skill scores, Q. J. R. Meteor. Soc., 140, 1889–1899, 2014.

Vitart, F., Buizza, R., Balmaseda, M. A., Balsamo, G., Bidlot, J.-R., Bonet, A., Fuentes, M., Hofstadler, A., Molteni, F., and Palmer, T.: The new VAREPS-monthly forecasting system: a first step towards seamless prediction, Q. J. R. Meteor. Soc., 134, 1789–1799, 2008.

Wennberg, P. O., Wunch, D., Roehl, C., Blavier, J.-F., Toon, G. C., Allen, N., Dowell, P., Teske, K., Martin, C., and Martin, J.: TCCON data from Lamont, Oklahoma, USA, Re-

lease GGG2014R0, Tech. rep., TCCON data archive, hosted by the Carbon Dioxide Information Analysis Center, Oak Ridge National Laboratory, Oak Ridge, Tennessee, USA, doi:10.14291/tccon.ggg2014.sodankyla01.R0/1149280, 2014.

Wunch, D., Toon, G. C., Blavier, J.-F. L., Washenfelder, R. A., Notholt, J., Connor, B., Griffith, D. W. T., Sherlock, V., and Wennberg, P. O.: The total carbon column observing network, P. T. R. Soc. A, 369, 2087–2112, doi:10.1098/rsta.2010.0240, 2011.

Table 1. Percentage of land grid points at model resolution TL255 ($\sim$ 80 km) for each dominant vegetation type, i.e. more than half of the grid point is covered by that vegetation type. A land grid point is defined by a land sea mask value greater than 0.5.

Vegetation Code	Vegetation type	Percentage of land points
1	Crops, Mixed Farming	9.9
2	Short Grass	7.6
7	Tall Grass	6.3
9	Tundra	6.3
10	Irrigated Crops	2.2
11	Semidesert	13.5
13	Bogs and Marshes	0.8
16	Evergreen Shrubs	0.5
17	Deciduous Shrubs	2.4
3	Evergreen Needle leaf Trees	5.7
4	Deciduous Needle leaf Trees	2.4
5	Deciduous Broadleaf Trees	4.0
6	Evergreen Broadleaf Trees	12.1
18	Mixed Forest/woodland	3.3
19	Interrupted Forest	9.5
21	Tropical Savanna (new type)	4.8
–	Remaining land points without vegetation	8.7

Table 2. List of simulations with the same transport and different CO_2 surface fluxes.

Experiment name	CO_2 surface fluxes
CTRL	Biogenic fluxes from CTESSEL (Boussetta et al., 2013), biomass burning fluxes from GFAS (Kaiser et al., 2012), ocean fluxes from Takahashi et al. (2009), and EDGAR v4.2 anthropogenic fluxes (Janssens-Maenhout et al., 2012)
OPT	MACC-13R1 optimised fluxes (Chevallier et al., 2010) for 2010
OPT-CLIM	MACC-13R1 optimised flux climatology (2004–2013)
BFAS	Same fluxes as CTRL including BFAS

Table 3. List of TCCON stations used in Fig. 10 ordered by latitude from North to South.

Site	Latitude [degrees]	Longitude [degrees]	Altitude [m a.s.l]	Reference
Sodankylä	67.37	26.63	190.0	Kivi et al. (2014)
Białystok	53.23	23.02	160.0	Deutscher et al. (2014)
Lamont	36.60	−97.49	320.0	Wennberg et al. (2014)
Wollongong	−34.41	150.88	30.0	Griffith et al. (2014)

Table 4. Correlation coefficient of different forecast (FC) experiments (see Table 2) with observations at three NOAA/ESRL tall towers for daily mean dry molar fraction of atmospheric CO_2 in March 2010. The dash symbol means the correlation is not significant.

NOAA/ESRL Tower site (ID)	Latitude, Longitude, Altitude	Sampling level [m]	BFAS FC	CTRL FC	OPT FC	OPT-CLIM FC
Park Falls,	45.95° N,	30	0.843	0.338	0.794	0.797
Wisconsin	90.27° W,	122	0.931	0.508	0.893	0.883
(LEF)	472 m	396	0.919	–	0.875	0.881
West Branch,	41.72° N,	31	0.748	0.496	0.590	0.590
Iowa	91.35° W,	99	0.833	0.436	0.767	0.720
(WBI)	242 m	379	0.851	0.356	0.887	0.876
Argyle,	45.03° N,	12	0.857	0.839	0.808	0.893
Maine	68.68° W,	30	0.875	0.835	0.816	0.938
(AMT)	50 m	107	0.861	0.668	0.816	0.927
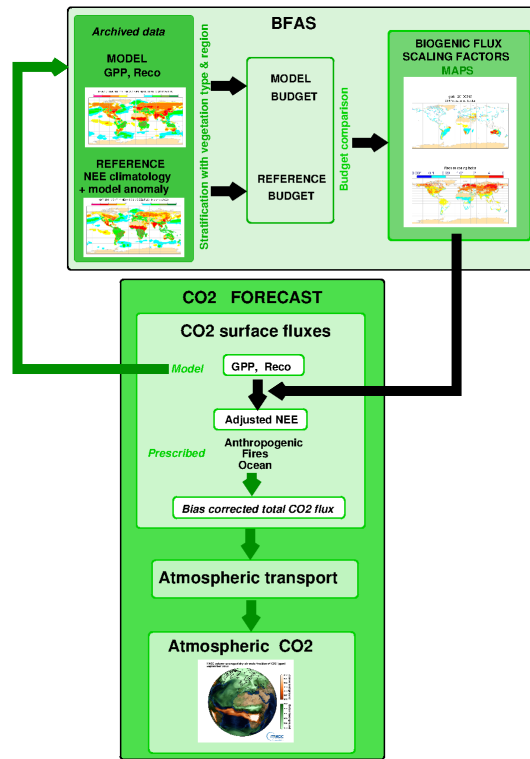
Figure 1. Schematic showing how BFAS fits in the atmospheric CO_2 forecasting system. BFAS is called before each forecast to compute the scaling factors for the model NEE (i.e. GPP $+R_{eco}$) based on the past archived forecasts. The maps of the scaling factors are then passed to the model which applies the adjustment to the output biogenic CO_2 fluxes from the land surface model. After combining the adjusted NEE fields with the other prescribed CO_2 fluxes, the resulting bias corrected fluxes are passed to the transport model to produce the atmospheric CO_2 forecast.
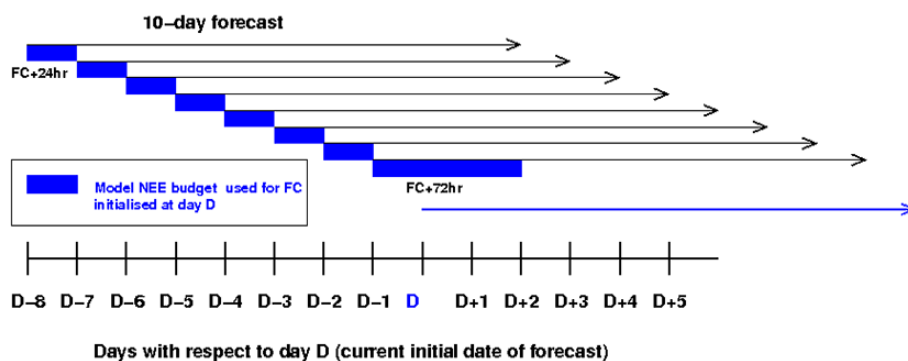
Figure 2. Schematic to illustrate how the 10-day NEE budget from the model is computed in BFAS for the forecast at day D by retrieving the past forecasts of accumulated NEE. Note that the retrieved NEE (computed by adding GPP and R_{eco}) has not been corrected by BFAS. The computation uses a set of 7 previous 1-day forecasts (initialised at $D-8$, $D-7$, $D-6$,... until $D-2$) together with the latest 3-day forecast from the previous day (i.e. $D-1$) as shown by the blue boxes.
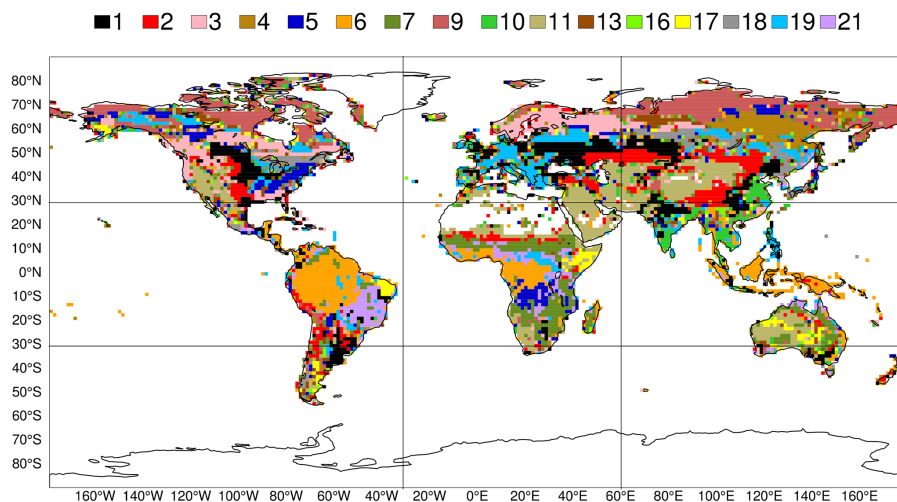
Figure 3. Dominant vegetation types based on the BATS classification used in the IFS and extended to include the tropical savanna subtype (in purple, as defined by the Olson (1994a) classification) within the interrupted forest type (in light blue). The vegetation type codes are described in Table 1. The nine regions used in the computation of the NEE budget are delimited by the black lines.
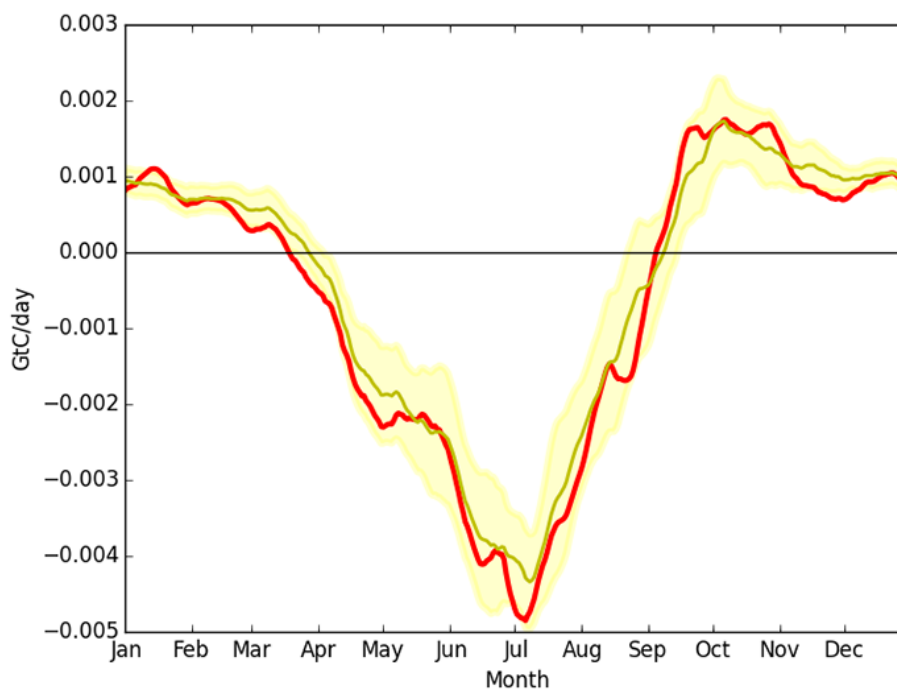
Figure 4. Time series of 10-day mean NEE budget [GtC/day] associated with the crop vegetation type in North America from the MACC-13R1 optimised flux data set in 2010 (red line) compared to its climatology (2004–2013) (yellow line). The yellow shading represents the standard deviation of the optimised flux budget (for the same period) used to compute the inter-annual variability adjustment applied to the reference climatology. Positive/negative values correspond to a source/sink of CO_2.
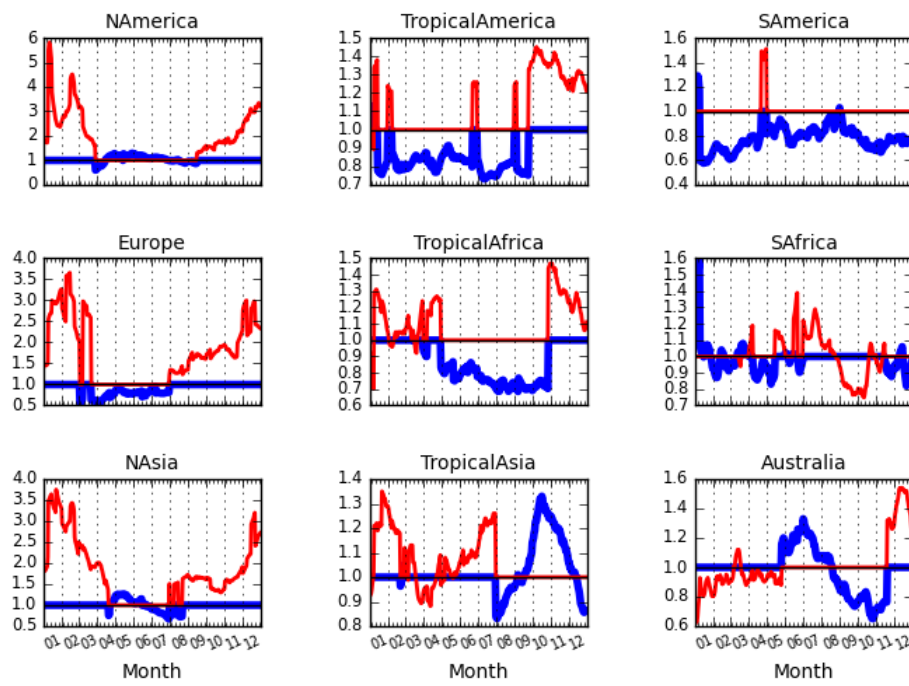
Figure 5. Time series of GPP and R_{eco} flux scaling factors in blue and red lines respectively for the crop vegetation type in 2010 in the different regions (see map in Fig. 3 depicting the extent of the crops within each region).

(a) GPP scaling factor

(b) Reco scaling factor
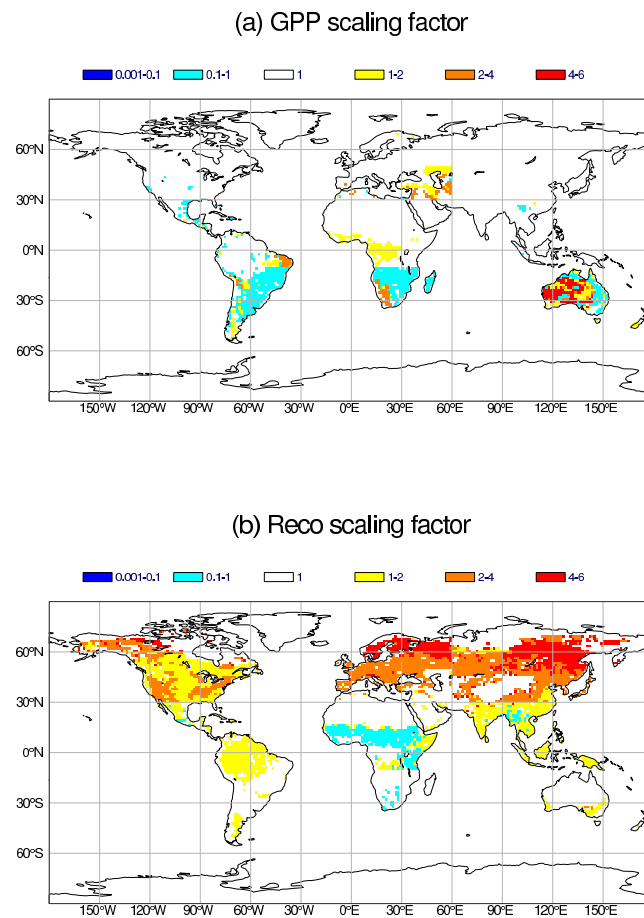
Figure 6. Map of scaling factors for **(a)** GPP and **(b)** R_{eco} on 15 March 2010.
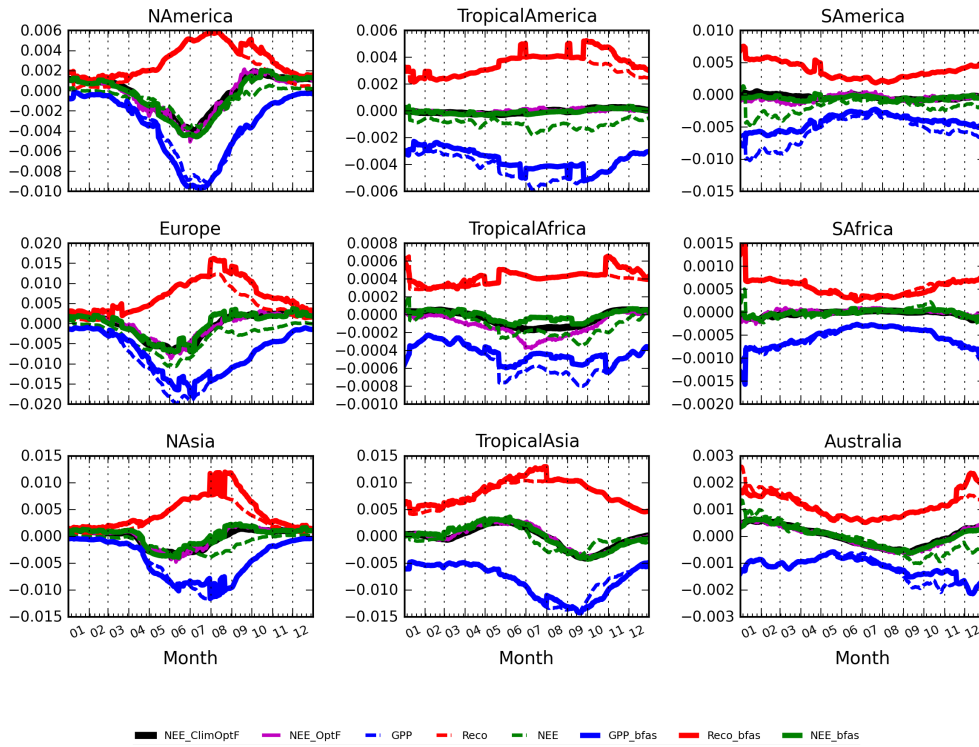
Figure 7. Time series of GPP (in blue), R_{eco} (in red) and NEE (in green) daily budget [GtC/day] before and after the flux adjustment (see dashed lines and solid lines respectively) for crops in 2010 in the different regions. The reference budget provided by the climatology of MACC-13R1 optimised fluxes (2004–2013) and the MACC-13R1 optimised fluxes for 2010 are depicted by the black and magenta lines respectively. Positive/negative values correspond to a source/sink of CO_2.
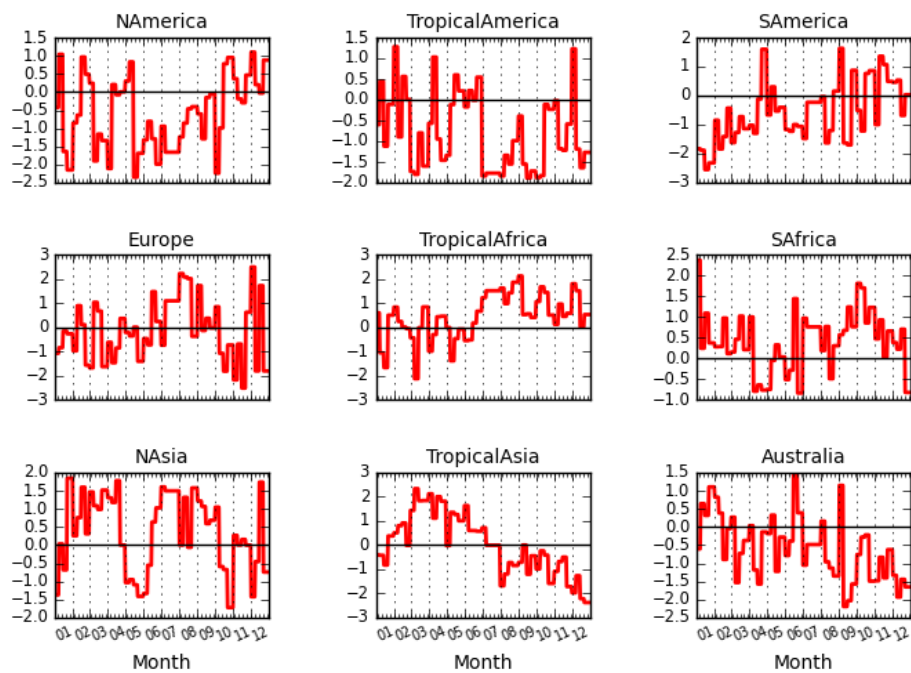
Figure 8. Time series of the standardised anomaly of the modelled NEE budget (γ in Eq. 3) for crops in 2010 in the different regions. Positive values indicate larger/smaller CO_2 sources/sinks than normal based on the mean climatological budget; whereas negative values correspond to smaller/larger CO_2 sources/sinks than normal.
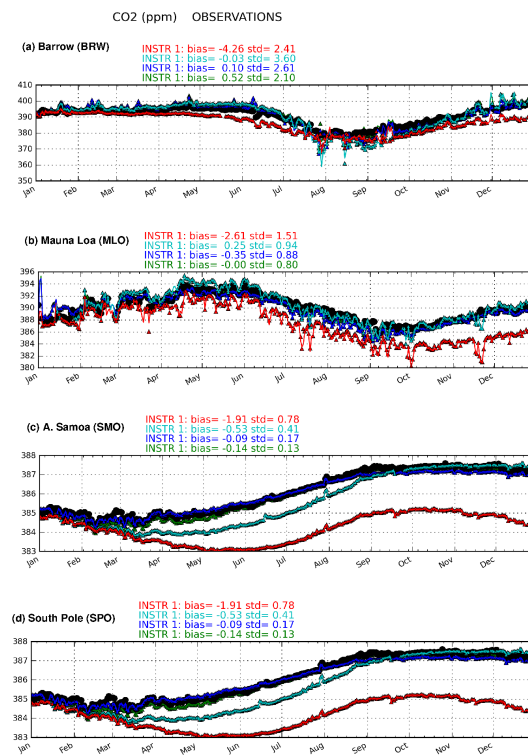
Figure 9. Daily mean atmospheric CO_2 dry molar fraction [ppm] from NOAA/ESRL continuous baseline stations (black circles) at **(a)** Barrow, Alaska, USA (71.32° N, 156.61° W), **(b)** Mauna Loa, Hawaii, US (19.54° N, 155.58° W), **(c)** Tutuila, American Samoa, USA (14.25° S, 170.56° W), **(d)** South Pole, Antarctica (89.98° S, 24.8° W) and the different forecast experiments: BFAS (cyan), CTRL (red), OPT (green) and OPT-CLIM (blue). See Table 2 for a description of the different experiments. The mean (bias) and standard deviation (SD) of the model errors are shown at the top of each panel.
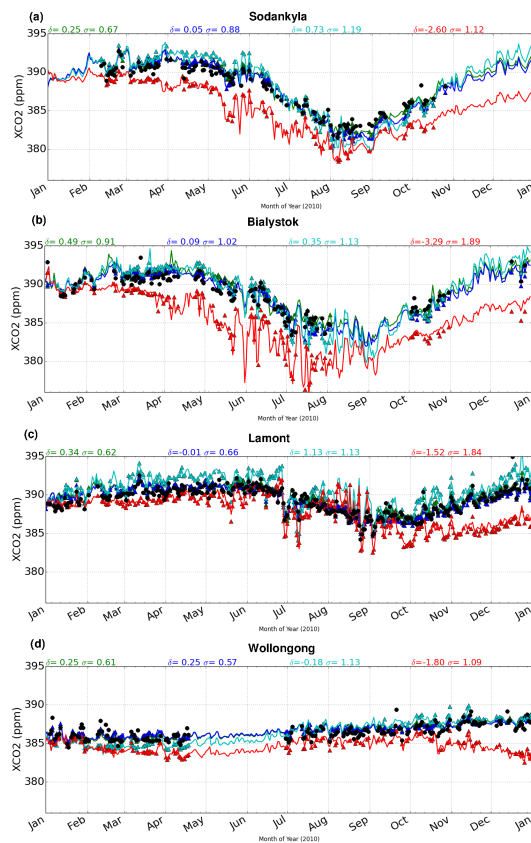
Figure 10. Daily mean atmospheric CO_2 column-average dry molar fraction [ppm] observed at four TCCON stations (see Table 3) as shown by the black circles, and simulated by the different forecast experiments: BFAS (cyan), CTRL (red), OPT (green) and OPT-CLIM (blue). See Table 2 for a description of the different experiments. The mean (δ) and standard deviation (σ) of the model errors are shown at the top of each panel.
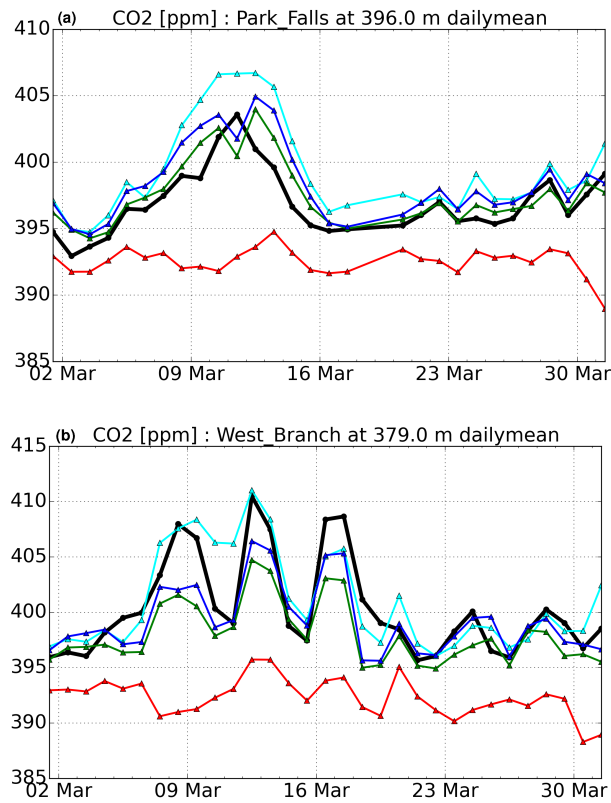
Figure 11. Daily mean atmospheric CO_2 dry molar fraction [ppm] in March 2010 from NOAA/ESRL tall towers (black circles) at **(a)** Park Falls (Wisconsin, USA, 45.95° N, 90.27° W) and **(b)** West Branch (Iowa, USA, 41.72° N, 91.35° W) and the different forecast experiments: BFAS (cyan), CTRL (red), OPT (green) and OPT-CLIM (blue) (see Table 2 for a description of the different experiments).
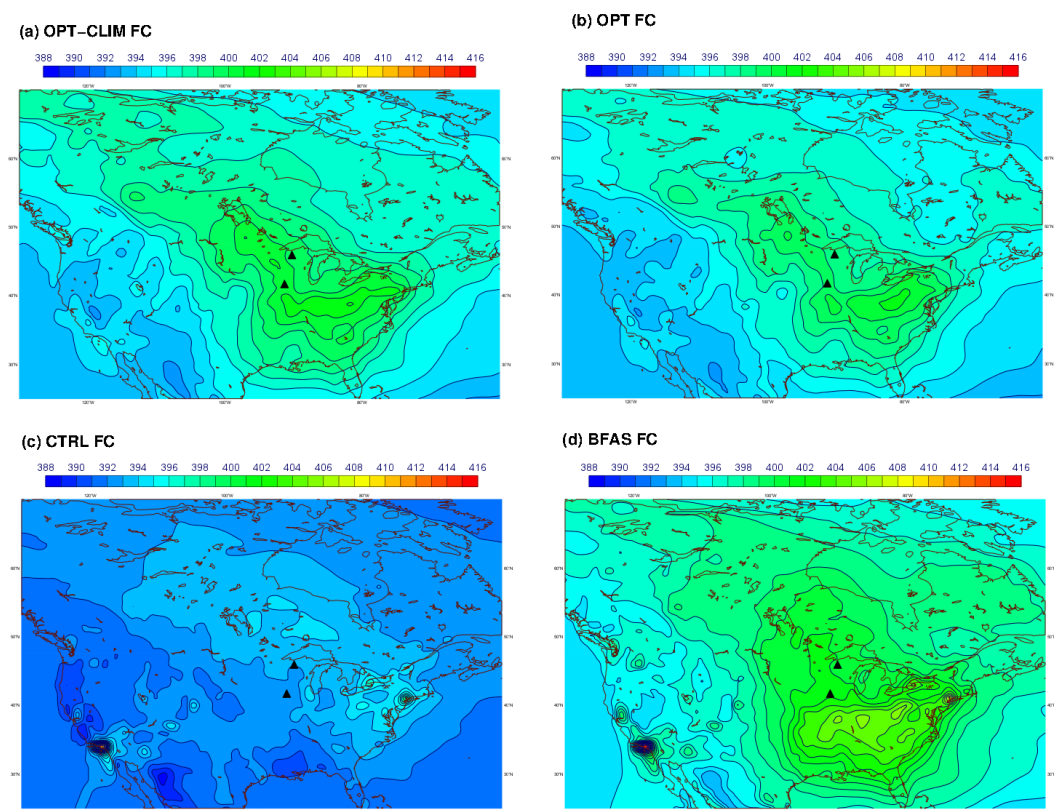
Figure 12. Monthly mean atmospheric CO_2 dry molar fraction [ppm] at the model level approximately corresponding to the highest sampling height of the Park Falls and West Branch NOAA/ESRL tall towers (see black triangles) in March 2010 from **(a)** OPT-CLIM, **(b)** OPT, **(c)** CTRL and **(d)** BFAS experiments (see Table 2 for a description of the different experiments).
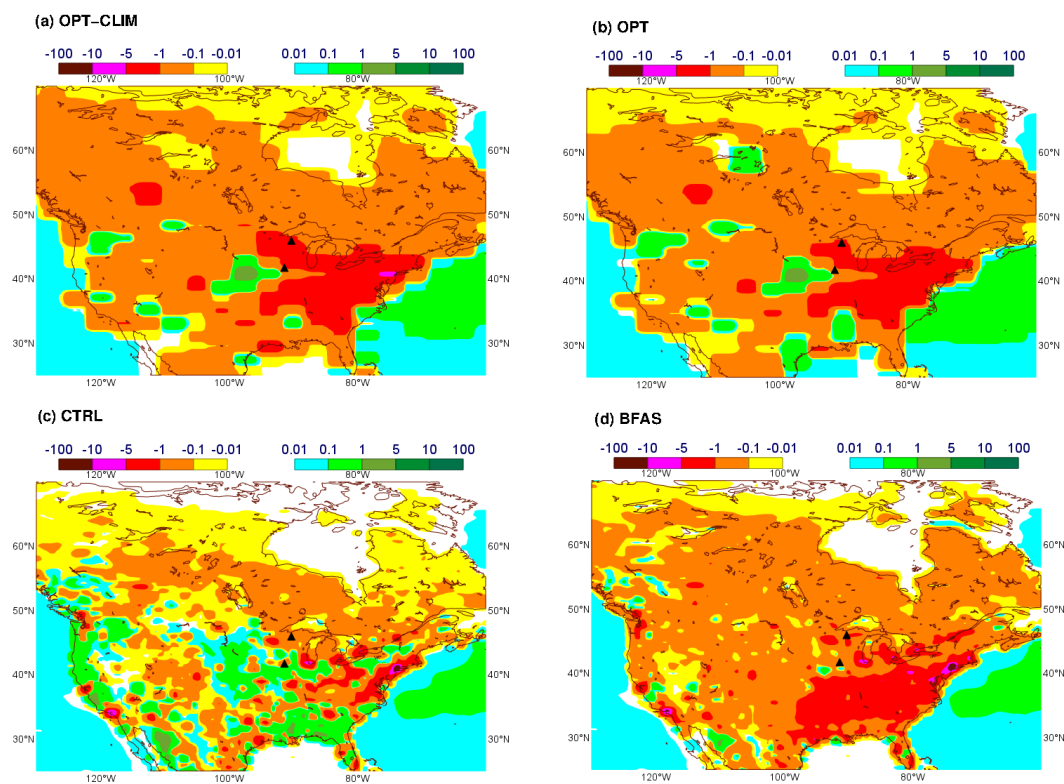
Figure 13. Monthly mean total CO_2 flux [μmol m^{-2} s^{-1}] in March 2010 from **(a)** OPT-CLIM, **(b)** OPT, **(c)** CTRL and **(d)** BFAS experiments (see Table 2 for a description of the different experiments). The black triangles depict the location of the NOAA/ESRL tall towers plotted in Fig. 11.